Contents lists available at ScienceDirect

Signal Processing

journal homepage: www.elsevier.com/locate/sigpro

Underdetermined direction-of-departure and direction-of-arrival estimation in bistatic multiple-input multiple-output radar ☆

Frankie K.W. Chan [a], H.C. So [a], Lei Huang [b,*], Long-Ting Huang [a]

[a] Department of Electronic Engineering, City University of Hong Kong, Hong Kong, China
[b] Department of Electronic and Information Engineering, Harbin Institute of Technology Shenzhen Graduate School, Shenzhen, China

ABSTRACT

In this paper, target localization using bistatic multiple-input multiple-output radar where the source number exceeds the sizes of the transmit and receive arrays, denoted by M and N, respectively, is addressed. We consider the Swerling II target in which the radar cross section varies in different pulses. Two algorithms for joint direction-of-departure (DOD) and direction-of-arrival (DOA) estimation of the targets are devised. The first one is a subspace-based estimator which is computationally simpler and can identify up to $2(M-1)(2N-1)$ sources, assuming that $N \geq M$. The second is a maximum likelihood method with a higher estimation accuracy, where the DODs and DOAs are solved via alternating optimization. Simulation results are included to compare their mean square error performance with the Cramér–Rao lower bound.

© 2014 Published by Elsevier B.V.

1. Introduction

The topic of source localization with the use of multiple-input multiple-output (MIMO) radar has received considerable interest [1–3]. The orthogonal waveforms emitted by the transmit antennas of the MIMO radar, when impinge on moving targets, will be reflected to its receive antennas. Unlike traditional phase array radar which uses coherent waveforms, MIMO radar simultaneously transmits multiple orthogonal signals and is able to offer superior performance.

Basically, there are two categories of MIMO radars, where statistical and colocated antennas are employed.

In the first class [2,4–6], the transmit antennas are widely separated compared with their distances to targets. Hence, the sources can be identified from different directions simultaneously, and spatial diversity gain of targets as well as high target resolution are achieved. The second type can be further classified as monostatic [7–10] and bistatic MIMO radars [11,12], where both of the elements of transmit and receive antennas are closely spaced compared to the target ranges. Their main difference is that the transmitters and receivers are close to each other in the first type of radar but they are separated away from each other in the bistatic counterpart. This leads to the consequence of same and distinct direction-of-departure (DOD) and direction-of-arrival (DOA) for each target in the former and latter, respectively. In this work, our task is to find the DODs and DOAs for locating multiple targets using the bistatic MIMO radar in the underdetermined scenario of $K > \max(M, N)$ where K, M and N represent the

* Corresponding author: Tel.: +86 75586011571.
E-mail addresses: kwfchan@gmail.com (F.K.W. Chan),
hcso@ee.cityu.edu.hk (H.C. So), dr.lei.huang@ieee.org (L. Huang),
huanglt08@gmail.com (L.-T. Huang).

numbers of targets, transmit antennas and receive antennas, respectively.

A number of underdetermined DOD and DOA estimation algorithms have been developed for the MIMO data model where the radar cross section (RCS) remains unchanged in all the pulses, namely, the Swerling I target. In the presence of white Gaussian noise, the optimum solution is obtained by finding the peak of the maximum likelihood (ML) cost function, and the corresponding $2K$-dimensional ($2K$-D) optimization problem can be broken down into $2K$ iterative 1-D searches [12]. To avoid large computational burden due to the highly nonlinear maximization, subspace methodology which exploits the signal and noise subspaces via eigenvalue decomposition of the sample covariance matrix or singular value decomposition (SVD) of the raw data matrix is a popular choice for suboptimal techniques. 2-D multiple signal classification (MUSIC) [13,14], which uses the noise subspace, has been suggested using double polynomial root finding procedure to estimate the DODs and DOAs. On the other hand, estimation of signal parameters via rotational invariance technique (ESPRIT) [11,15,16], which employs the signal subspace, is able to produce closed-form DOD and DOA estimates with auto-pairing. In this work, we consider a fast changing environment when the RCSs are different among the pulses. That is, Swerling II target model is adopted [17,18]. The transmit and receive antenna configurations are assumed to be uniform linear array (ULA). Under this setting, the number of identifiable targets is nearly four times that of the model with identical RCSs. Two joint DOD and DOA estimation algorithms where the first is a computationally efficient ESPRIT-like algorithm and the second is a ML estimator with high estimation accuracy, will be devised.

The rest of this paper is organized as follows. In Section 2, the data model and problem formulation are presented. The ESPRIT method is developed and its identifiability is analyzed in Section 3. In Section 4, the ML estimator is derived and we propose to apply alternating optimization to solve for the DODs and DOAs with the ESPRIT solution being the initial estimate. In Section 5, the localization performance of the two algorithms is evaluated by comparing with the Cramér–Rao lower bound (CRLB). Finally, conclusions are drawn in Section 6.

Throughout this paper, we use boldface uppercase letters to denote matrices, boldface lowercase letters for column vectors, and lowercase letters for scalar quantities. Superscripts $(\cdot)^*$, $(\cdot)^T$, $(\cdot)^H$, $(\cdot)^{-1}$ and $(\cdot)^\dagger$ represent complex conjugate, transpose, Hermitian transpose, matrix inverse, and pseudo inverse, respectively. The gradient of $f(\mathbf{a})$ with respect to $\mathbf{a}$ is denoted by $\nabla_{\mathbf{a}}f$. The $\Re\alpha$ and $\Im\alpha$ denote the real part and complex part of a. Moreover, $\hat{a}$ denotes the estimate of a and $E\{a\}$ is the expected value of a. The $[\mathbf{A}]_{m,n}$ represents the (m,n) entry of $\mathbf{A}$, while tr($\mathbf{A}$) and $|\mathbf{A}|$ are the trace and determinant of $\mathbf{A}$, respectively. The block diagonal matrix, with $\mathbf{A}_1$ and $\mathbf{A}_2$ being its components, is denoted by diag$(\mathbf{A}_1, \mathbf{A}_2)$, and vec($\mathbf{A}$) is the columnwise vectorized version of $\mathbf{A}$. The Kronecker product and Khatri-Rao matrix product are denoted by $\otimes$ and $\circ$, respectively. Furthermore, $\mathbf{I}_M$ is the $M \times M$ identity matrix, $\mathbf{1}_M$ is the $M \times 1$ vector with all elements equal one and $\mathbf{0}_M$ is the $M \times 1$ zero vector. The $\mathbf{x} \sim \mathcal{CN}(\boldsymbol{\mu}, \boldsymbol{\Sigma})$ means that $\mathbf{x}$ is complex Gaussian distributed with mean $\boldsymbol{\mu}$ and covariance matrix $\boldsymbol{\Sigma}$.

2. Signal model and problem formulation

Consider a bistatic MIMO radar system with an M-element transmit and an N-element receive ULAs for locating K targets in the range bin of interest. The emitted signal impinges on the targets and the pth reflected pulse signal arrived at the receive antennas, after matched filtering, can be expressed as

$$\mathbf{X}_p = \mathbf{FS}_p + \mathbf{Q}_p, \quad p = 1, 2, \ldots, P \tag{1}$$

where

$$\mathbf{F} = \mathbf{H} \circ \mathbf{G} \in \mathbb{C}^{MN \times K} \tag{2}$$

$$\mathbf{G} = [\mathbf{g}_1 \ \mathbf{g}_2 \ \cdots \ \mathbf{g}_K] \in \mathbb{C}^{M \times K} \tag{3}$$

$$\mathbf{H} = [\mathbf{h}_1 \ \mathbf{h}_2 \ \cdots \ \mathbf{h}_K] \mathbb{C}^{N \times K} \tag{4}$$

$$\mathbf{g}_k = \left[1 \ \exp\left\{ j\frac{2\pi d_t \sin(\breve{\theta}_k)}{\lambda} \right\} \ \cdots \ \exp\left\{ j\frac{2\pi d_t(M-1)\sin(\breve{\theta}_k)}{\lambda} \right\} \right]^T \tag{5}$$

$$\mathbf{h}_k = \left[1 \ \exp\left\{ j\frac{2\pi d_r \sin(\breve{\phi}_k)}{\lambda} \right\} \ \cdots \ \exp\left\{ j\frac{2\pi d_r(N-1)\sin(\breve{\phi}_k)}{\lambda} \right\} \right]^T. \tag{6}$$

The $\breve{\theta}_k \in (-\pi/2, \pi/2)$ and $\breve{\phi}_k \in (-\pi/2, \pi/2)$ denote the DOD and DOA of the kth target to be estimated, respectively. Furthermore, λ is the carrier wavelength while d_t and d_r are the inter-element separations in the transmitter and receiver, and they are known constants. A total of P pulses in the interesting range bin are collected, and in each pulse, there are L samples or snapshots. In this work, we consider the underdetermined scenario of $\max(M,N) < K \leq \min(L,P)$. The $[\mathbf{S}_p]_{k,\ell}$ is RCS of the ℓth snapshot within the pth pulse of the kth target. It is assumed that the distribution of the RCS of the kth target is the same for snapshots within pulses but different among pulses, that is, $[\mathbf{S}_p]_{k,\ell} \sim \mathcal{N}(0, \ \alpha_{k,p}^2)$, $p = 1, 2, \ldots, P$, $k = 1, 2, \ldots, K$, $\ell = 1, 2, \ldots, L$. The (k, ℓ) entry of $\mathbf{Q}_p$ is the zero-mean white Gaussian noise of the kth target at the ℓth snapshot in the pth pulse, which is independent among snapshots, pulses and targets, and we can write $[\text{vec}(\mathbf{Q}_1)^T \ \text{vec}(\mathbf{Q}_2)^T \ \cdots \ \text{vec}(\mathbf{Q}_P)^T]^T \sim \mathcal{CN}(\mathbf{0}_{MNLP \times 1}, \ \sigma^2\mathbf{I}_{MNLP})$. The values of $\{\alpha_{k,p}^2\}$ and σ^2 are unknown. Note that (1)–(6) correspond to the Swerling II [19] target model where the RCS varies in different pulses. For the ease of presentation, we convert the DODs and DOAs to spatial frequencies by letting $\theta_k = 2\pi d_t \sin(\breve{\theta}_k)/\lambda$ and $\phi_k = 2\pi d_r \sin(\breve{\phi}_k)/\lambda$. Since d_t, d_r and λ are known and $-\pi/2 < \breve{\theta}_k, \breve{\phi}_k < \pi/2$, we can straightforwardly determine the DODs and DOAs once θ_k and ϕ_k are estimated.

3. ESPRIT-like estimator

Let $\mathbf{x}_{p,\ell} \in \mathbb{C}^{MN}$ be the ℓth column of $\mathbf{X}_p$, that is,

$$\mathbf{X}_p = [\mathbf{x}_{p,1} \ \mathbf{x}_{p,2} \ \cdots \ \mathbf{x}_{p,L}]. \tag{7}$$

The covariance matrix of the pth pulse, denoted by $\mathbf{R}_p$, $p = 1, 2, ..., P$, is easily shown to be

$$\mathbf{R}_p = \frac{1}{L} E\{\mathbf{X}_p \mathbf{X}_p^H\} = \frac{1}{L} \sum_{\ell=1}^{L} E\{\mathbf{x}_{p,\ell} \, \mathbf{x}_{p,\ell}^H\} = \mathbf{F} \operatorname{diag}(\boldsymbol{\alpha}_p) \mathbf{F}^H + \sigma^2 \mathbf{I}_{MN} \tag{8}$$

where

$$\boldsymbol{\alpha}_p = [\alpha_{1,p} \; \alpha_{2,p} \; \cdots \; \alpha_{K,p}]^T. \tag{9}$$

Our first step is to compute the ranks of several matrices in order to determine the signal subspace of the ESPRIT estimator. When noise is absent or $\sigma^2 = 0$, vectorizing $\mathbf{R}_p$ yields

$$\operatorname{vec}(\mathbf{R}_p) = (\mathbf{F}^* \circ \mathbf{F}) \boldsymbol{\alpha}_p, \quad p = 1, 2, ..., P. \tag{10}$$

Stacking the P vectors in (10), we obtain

$$\mathcal{R} \triangleq [\operatorname{vec}(\mathbf{R}_1) \; \operatorname{vec}(\mathbf{R}_2) \; \cdots \; \operatorname{vec}(\mathbf{R}_P)] = (\mathbf{F}^* \circ \mathbf{F}) \mathbf{A} \in \mathbb{C}^{(MN)^2 \times P} \tag{11}$$

where

$$\mathbf{A} = [\boldsymbol{\alpha}_1 \; \boldsymbol{\alpha}_2 \; \cdots \; \boldsymbol{\alpha}_P]. \tag{12}$$

As $\mathbf{A} \in \mathbb{R}^{K \times P}$ is drawn randomly from a distribution where $K < P$, it has full rank with probability one. As a result, the rank of $(\mathbf{F}^* \circ \mathbf{F}) \mathbf{A}$ equals that of $\mathbf{F}^* \circ \mathbf{F}$. The rank of $\mathbf{F}^* \circ \mathbf{F}$ is now investigated.

Lemma 1. *There exists a permutation matrix* $\mathbf{J} \in \{0, 1\}^{M^2 N^2 \times M^2 N^2}$ *such that*

$$\mathbf{F}^* \circ \mathbf{F} = \mathbf{J}(\mathbf{H}^* \circ \mathbf{H} \circ \mathbf{G}^* \circ \mathbf{G}). \tag{13}$$

Proof of Lemma 1. There exists a permutation matrix $\tilde{\mathbf{J}} \in \{0, 1\}^{MN \times MN}$ such that $\mathbf{G}^* \circ \mathbf{H} = \tilde{\mathbf{J}}(\mathbf{H} \circ \mathbf{G}^*)$. We then have

$$\mathbf{F}^* \circ \mathbf{F} = (\mathbf{H}^* \circ (\tilde{\mathbf{J}}(\mathbf{H} \circ \mathbf{G}^*)) \circ \mathbf{G} = \mathbf{J}(\mathbf{H}^* \circ \mathbf{H} \circ \mathbf{G}^* \circ \mathbf{G}) \tag{14}$$

where

$$\mathbf{J} = \mathbf{I}_N \otimes \tilde{\mathbf{J}} \otimes \mathbf{I}_M. \tag{15}$$

From Lemma 1, the rank of $\mathbf{F}^* \circ \mathbf{F}$ equals that of $\mathbf{H}^* \circ \mathbf{H} \circ \mathbf{G}^* \circ \mathbf{G}$. Therefore, we now investigate the ranks of $\mathbf{G}^* \circ \mathbf{G}$ and $\mathbf{H}^* \circ \mathbf{H}$.

Lemma 2.

$$\mathbf{G}^* \circ \mathbf{G} = \mathcal{L}_G \mathcal{G} \tag{16}$$

where

$$\mathcal{G} = \begin{bmatrix} e^{j(1-M)\theta_1} & e^{j(1-M)\theta_2} & \cdots & e^{j(1-M)\theta_K} \\ e^{j(2-M)\theta_1} & e^{j(2-M)\theta_2} & \cdots & e^{j(2-M)\theta_K} \\ \vdots & \vdots & \ddots & \vdots \\ e^{j(M-1)\theta_1} & e^{j(M-1)\theta_2} & \cdots & e^{j(M-1)\theta_K} \end{bmatrix} \in \mathbb{C}^{(2M-1) \times K} \tag{17}$$

and $\mathcal{L}_G \in \{0, 1\}^{M^2 \times (2M-1)}$.

Proof of Lemma 2. The kth column of $\mathbf{G}^* \circ \mathbf{G}$ is $\mathbf{g}_k^* \otimes \mathbf{g}_k$, which equals $\operatorname{vec}(\mathbf{g}_k \mathbf{g}_k^H)$. As $\mathbf{g}_k \mathbf{g}_k^H \in \mathbb{C}^{M \times M}$ is Hermitian Toeplitz with first column and first row being $\mathbf{g}_k \in \mathbb{C}^M$ and $\mathbf{g}_k^H$, respectively. Therefore, $\mathbf{g}_k^* \otimes \mathbf{g}_k \in \mathbb{C}^{M^2}$ has only $(2M-1)$ distinct entries.

Corollary 1.

$$\mathbf{H}^* \circ \mathbf{H} = \mathcal{L}_H \mathcal{H} \tag{18}$$

where

$$\mathcal{H} = \begin{bmatrix} e^{j(1-N)\phi_1} & e^{j(1-N)\phi_2} & \cdots & e^{j(1-N)\phi_K} \\ e^{j(2-N)\phi_1} & e^{j(2-N)\phi_2} & \cdots & e^{j(2-N)\phi_K} \\ \vdots & \vdots & \ddots & \vdots \\ e^{j(N-1)\phi_1} & e^{j(N-1)\phi_2} & \cdots & e^{j(N-1)\phi_K} \end{bmatrix} \in \mathbb{C}^{(2N-1) \times K} \tag{19}$$

and $\mathcal{L}_H \in \{0, 1\}^{N^2 \times (2N-1)}$.

Based on Lemma 2 and Corollary 1, we have

Lemma 3. *The rank of* $\mathbf{H}^* \circ \mathbf{H} \circ \mathbf{G}^* \circ \mathbf{G}$ *equals that of* $\mathcal{H} \circ \mathcal{G}$.

Proof of Lemma 3. By (16) and (18), we have

$$\mathbf{H}^* \circ \mathbf{H} \circ \mathbf{G}^* \circ \mathbf{G} = \mathcal{L}(\mathcal{H} \circ \mathcal{G}) \tag{20}$$

where

$$\mathcal{L} = \mathcal{L}_H \otimes \mathcal{L}_G. \tag{21}$$

As $\mathcal{L} \in \{0, 1\}^{(M^2 N^2) \times (2M-1)(2N-1)}$ has rank $(2M-1)(2N-1)$, the rank of $\mathbf{H}^* \circ \mathbf{H} \circ \mathbf{G}^* \circ \mathbf{G}$ equals that of $\mathcal{H} \circ \mathcal{G}$.

From (17) and (19), $\mathcal{G} \in \mathbb{C}^{(2M-1) \times K}$ and $\mathcal{H} \in \mathbb{C}^{(2N-1) \times K}$ are Vandermonde matrices and the following theorem specifies the rank of $\mathcal{H} \circ \mathcal{G}$, which is also the rank of $\mathbf{F}^* \circ \mathbf{F}$.

Theorem 1. *If* θ_k *and* ϕ_k *are sampled from a distribution that is continuous with respect to the Lebesgue measure in* $\mathbb{C}^{2K}$, *then the rank of* $\mathcal{H} \circ \mathcal{G}$ *is* $\min((2M-1)(2N-1), K)$ *almost surely.*

Proof of Theorem 1. See [20, p. 45].

In the presence of noise or $\sigma^2 > 0$, we employ (8), (11), (13) and (20) to obtain

$$\mathcal{R} = \mathbf{J}\mathcal{L}(\mathcal{H} \circ \mathcal{G})\mathbf{A} + \sigma^2 \imath_{MN} \mathbf{1}_P^T \tag{22}$$

where

$$\imath_{MN} = \operatorname{vec}(\mathbf{I}_{MN}) \tag{23}$$

To remove the noise component, we post-multiply (22) by the null space of $\mathbf{1}_P^T$, denoted by $(\mathbf{1}_P^T)^\perp$. Together with pre-multiplication of the pseudo inverse of $\mathbf{J}\mathcal{L}$, a modified covariance matrix is constructed as

$$\mathcal{R} \triangleq (\mathbf{J}\mathcal{L})^\dagger \mathcal{R}(\mathbf{1}_P^T)^\perp = (\mathcal{H} \circ \mathcal{G})\mathbf{A}(\mathbf{1}_P^T)^\perp \in \mathbb{C}^{(2M-1)(2N-1) \times (P-1)}. \tag{24}$$

As $P - 1 \geq K$, the matrix $\mathbf{A}(\mathbf{1}_P^T)^\perp \in \mathbb{C}^{K \times (P-1)}$ has rank K with probability one. As a result, the rank of $\mathcal{R}$ equals that of $\mathcal{H} \circ \mathcal{G}$. By Theorem 1, $\mathcal{R}$ has rank K because $K \leq (2M-1)(2N-1)$. According to SVD, $\mathcal{R}$ can be decomposed as

$$\mathcal{R} = \mathbf{U}_s \operatorname{diag}(\lambda_1, \lambda_2 ..., \lambda_K) \mathbf{U}_s^H + \mathbf{U}_n \operatorname{diag}(\lambda_{K+1}, \lambda_{K+2} ..., \lambda_{P-1}) \mathbf{U}_n^H \tag{25}$$

where

$$\lambda_1 \geq \lambda_2 \geq \cdots \geq \lambda_K > \lambda_{K+1} = \cdots = \lambda_{P-1} = 0. \tag{26}$$

Here, $\mathbf{U}_s \in \mathbb{C}^{(2M-1)(2N-1) \times K}$ and $\mathbf{U}_n \in \mathbb{C}^{(2M-1)(2N-1) \times (MN-K)}$ represent the signal and noise subspaces, respectively, and $\lambda_1, \lambda_2, ..., \lambda_{P-1}$, are the corresponding singular values. It is

clear that the kth column of $[\mathbf{U}_s\ \mathbf{U}_n]$ is the singular vector corresponds to λ_k.

Nevertheless, we only have the sample covariance matrices which are computed as $\hat{\mathbf{R}}_p = \mathbf{X}_p\mathbf{X}_p^H/L$, $p = 1, 2, \ldots, P$. That is to say, in practice, $\mathbf{U}_s$ is computed from

$$\hat{\mathcal{R}} = (\mathbf{JL})^{\dagger}\hat{\mathcal{R}}(\mathbf{1}_P^T)^{\perp} \tag{27}$$

where $\hat{\mathcal{R}} = [\text{vec}(\hat{\mathbf{R}}_1)\ \text{vec}(\hat{\mathbf{R}}_2)\ \cdots\ \text{vec}(\hat{\mathbf{R}}_P)]$ and now $\hat{\lambda}_1 \geq \hat{\lambda}_2 \geq \hat{\lambda}_K > \hat{\lambda}_{K+1} \geq \cdots \geq \hat{\lambda}_{P-1} > 0$ where $\hat{\lambda}_k$ denotes the singular values of $\hat{\mathcal{R}}$.

After obtaining $\mathbf{U}_s$, we utilize the ESPRIT technique for parameter estimation by constructing four submatrices, namely, $\mathcal{Z}_1 \in \mathbb{C}^{2(M-1)(2N-1)\times K}$, $\mathcal{Z}_2 \in \mathbb{C}^{2(M-1)(2N-1)\times K}$, $\mathcal{Z}_3 \in \mathbb{C}^{2(N-1)(2M-1)\times K}$ and $\mathcal{Z}_4 \in \mathbb{C}^{2(N-1)(2M-1)\times K}$ as follows. Let $\mathbf{\Xi}$ be an index matrix

$$\mathbf{\Xi} = \begin{bmatrix} 1 & 2M & \cdots & (2M-1)(2N-1)-2M+2 \\ 2 & 2M+1 & \cdots & (2M-1)(2N-1)-2M+3 \\ \vdots & \vdots & \ddots & \vdots \\ 2M-1 & 4M-2 & \cdots & (2M-1)(2N-1). \end{bmatrix} \tag{28}$$

Then, $\mathcal{Z}_1$ and $\mathcal{Z}_2$ are the same as $\mathbf{U}_s$ except that the rows indexed by the last row and first row of $\mathbf{\Xi}$ being removed, respectively. Furthermore, $\mathcal{Z}_3$ and $\mathcal{Z}_4$ are the same as $\mathbf{U}_s$ except that the rows indexed by the last column and first column of $\mathbf{\Xi}$ being removed, respectively. In doing so, two equations are formed

$$\mathcal{Z}_1\mathbf{\Omega} \approx \mathcal{Z}_2 \tag{29}$$

and

$$\mathcal{Z}_3\mathbf{\Gamma} \approx \mathcal{Z}_4 \tag{30}$$

where the phase angles of the eigenvalues of $\mathbf{\Omega}$ and $\mathbf{\Gamma}$ are θ_k and ϕ_k, $k = 1, 2, \ldots, K$, respectively. The least squares (LS) estimates of $\mathbf{\Omega}$ and $\mathbf{\Gamma}$ are easily determined as

$$\hat{\mathbf{\Omega}} = \mathcal{Z}_1^{\dagger}\mathcal{Z}_2 \tag{31}$$

and

$$\hat{\mathbf{\Gamma}} = \mathcal{Z}_3^{\dagger}\mathcal{Z}_4 \tag{32}$$

For auto-pairing, the eigenvalues and eigenvectors of $\hat{\mathbf{\Omega}}$ are first calculated, that is, $\hat{\mathbf{\Omega}} = \mathbf{TCT}^{-1}$ where the columns of $\mathbf{T}$ are eigenvectors and $\mathbf{C}$ is the diagonal matrix of eigenvalues. Then, we compute $\mathbf{T}^{-1}\hat{\mathbf{\Gamma}}\mathbf{T}$ whose angle of the kth diagonal element is the estimate of ϕ_k and automatically paired up with that of θ_k. Alternatively, joint DOD and DOA estimation can be achieved by constructing a matrix $\mathbf{V}$ of the form

$$\mathbf{V} = \tilde{\mathbf{\Omega}} + j\tilde{\mathbf{\Gamma}} \tag{33}$$

where

$$\tilde{\mathbf{\Omega}} = j(\mathbf{I}_K + \hat{\mathbf{\Omega}})^{-1}(\mathbf{I}_K - \hat{\mathbf{\Omega}}) \tag{34}$$

$$\tilde{\mathbf{\Gamma}} = j(\mathbf{I}_K + \hat{\mathbf{\Gamma}})^{-1}(\mathbf{I}_K - \hat{\mathbf{\Gamma}}). \tag{35}$$

Then, $\hat{\theta}_k$ and $\hat{\phi}_k$ are obtained from the eigenvalues of $\mathbf{V}$, denoted by v_k, $k = 1, 2, \ldots, K$, as

$$\hat{\theta}_k = 2\tan^{-1}(\Re(v_k)) \tag{36}$$

$$\hat{\phi}_k = 2\tan^{-1}(\Im(v_k)). \tag{37}$$

From (36) and (37), the DODs and DOAs are automatically paired up. Employing the angle estimates to construct the approximate forms of $\mathcal{G}$ and $\mathcal{H}$, denoted by $\hat{\mathcal{G}}$ and $\hat{\mathcal{H}}$, we can compute $\mathbf{A}$ and σ^2 as follows. Using (22) and vectorization, we have

$$\text{vec}(\hat{\mathcal{R}}) \approx \mathbf{I}_P \otimes (\mathbf{JL}(\hat{\mathcal{H}}\circ\hat{\mathcal{G}}))\text{vec}(\mathbf{A}) + \sigma^2\mathbf{1}_P^T \otimes \iota_{MN}$$
$$= [\mathbf{I}_P \otimes (\mathbf{JL}(\hat{\mathcal{H}}\circ\hat{\mathcal{G}}))\ \mathbf{1}_P^T \otimes \iota_{MN}]\begin{bmatrix} \text{vec}(\mathbf{A}) \\ \sigma^2 \end{bmatrix}. \tag{38}$$

The LS estimates of $\mathbf{A}$ and σ^2 are then

$$\begin{bmatrix} \text{vec}(\hat{\mathbf{A}})^2 \\ \hat{\sigma} \end{bmatrix} = [\mathbf{I}_P \otimes (\mathbf{JL}(\hat{\mathcal{H}}\circ\hat{\mathcal{G}}))\ \mathbf{1}_P^T \otimes \iota_{MN}]^{\dagger}\text{vec}(\hat{\mathcal{R}}). \tag{39}$$

To guarantee unambiguous angle estimation, (29) and (30) indicate that the column lengths of $\mathcal{Z}_1$, $\mathcal{Z}_2$, $\mathcal{Z}_3$ and $\mathcal{Z}_4$ should be equal to or larger than those of the corresponding rows. Recall $\mathcal{Z}_1$, $\mathcal{Z}_2 \in \mathbb{C}^{2(M-1)(2N-1)\times K}$ and $\mathcal{Z}_3$, $\mathcal{Z}_4 \in \mathbb{C}^{2(N-1)(2M-1)\times K}$, the maximum number of targets that can be identified is thus equal to $2(M-1)(2N-1)$, assuming that $N \geq M$. Since performing SVD on $\hat{\mathcal{R}}$ corresponds to the major computational load, the complexity of the ESPRIT algorithm is $\mathcal{O}(P^3)$. It is worth pointing out that apart from ESPRIT, joint DOD and DOA estimation can also be achieved by applying the MUSIC algorithm on $\hat{\mathcal{R}}$.

4. Maximum likelihood estimator

In the following, the ML estimates of $\boldsymbol{\theta}$ and $\boldsymbol{\phi}$ are obtained using alternating optimization. First, let $\boldsymbol{x}_{\ell}$ be the vector collecting the ℓth snapshot of all pulses, that is, $\boldsymbol{x}_{\ell} = [\mathbf{x}_{1,\ell}^T\ \mathbf{x}_{2,\ell}^T\ \cdots\ \mathbf{x}_{P,\ell}^T]^T$. To derive the ML estimator, the first step is to construct the probability density function (PDF) of $\boldsymbol{x}_{\ell}$:

$$p(\boldsymbol{x}_{\ell}) = \pi^{-MNP}|\mathbf{R}|^{-1} + \exp\{-\boldsymbol{x}_{\ell}^H\mathbf{R}^{-1}\boldsymbol{x}_{\ell}\} \tag{40}$$

where

$$\mathbf{R} = \text{diag}(\mathbf{R}_1, \mathbf{R}_2, \ldots, \mathbf{R}_P) \tag{41}$$

Note that $\mathbf{R}$ is block diagonal as $\mathbf{S}_p$ and $\mathbf{Q}_p$ are uncorrelated. The joint PDF of $\boldsymbol{x}_1, \boldsymbol{x}_2, \ldots, \boldsymbol{x}_L$, which are independent, is

$$p(\boldsymbol{x}_1, \boldsymbol{x}_2, \ldots, \boldsymbol{x}_L) = \prod_{\ell=1}^{L} p(\boldsymbol{x}_{\ell}). \tag{42}$$

Taking logarithm on both sides yields

$$\log(p(\boldsymbol{x}_1, \boldsymbol{x}_2, \ldots, \boldsymbol{x}_L)) = -L(MNP\log(\pi) + \log(|\mathbf{R}|))$$
$$- \sum_{\ell=1}^{L} \boldsymbol{x}_{\ell}^H\mathbf{R}^{-1}\boldsymbol{x}_{\ell}. \tag{43}$$

Let $\boldsymbol{\theta} = [\theta_1\ \theta_2\ \cdots\ \theta_K]^T$ and $\boldsymbol{\phi} = [\phi_1\ \phi_2\ \cdots\ \phi_K]^T$. Dividing both sides by L and removing the constant term yields

$$-f(\boldsymbol{\theta}, \boldsymbol{\phi}, \mathbf{A}, \sigma^2) = \log(|\mathbf{R}|) + \frac{1}{L}\sum_{\ell=1}^{L}\text{tr}\left(\mathbf{R}^{-1}\boldsymbol{x}_{\ell}\ \boldsymbol{x}_{\ell}^H\right)$$
$$= \sum_{p=1}^{P}\log(|\mathbf{R}_p|) + \frac{1}{L}\sum_{\ell=1}^{L}\sum_{p=1}^{P}\text{tr}\left(\mathbf{R}_p^{-1}\mathbf{x}_{p,\ell}\ \mathbf{x}_{p,\ell}^H\right)$$
$$= \sum_{p=1}^{P}(\log(|\mathbf{R}_p|) + \text{tr}(\mathbf{R}_p^{-1}\hat{\mathbf{R}}_p)) \tag{44}$$

where

$$\hat{\mathbf{R}}_p = \frac{1}{L} \sum_{\ell=1}^{L} \mathbf{x}_{p,\ell} \, \mathbf{x}_{p,\ell}^H. \qquad (45)$$

In the following, $f(\theta, \phi, \mathbf{A}, \sigma^2)$ is replaced by f for brevity. Maximizing the ML cost function in (42) is equivalent to minimizing f. To avoid the extremely demanding $(2K+KP+1)$-D search, we propose to utilize alternating optimization as follows. First, we construct $\mathbf{F}$ with the use of estimates of θ and ϕ to find $\mathbf{A}$ and σ^2. Then, the estimates of $\mathbf{A}$ and σ^2 are treated as known parameters to update $\hat{\theta}$ and $\hat{\phi}$. Iterations between these two sets of parameters are performed until a stopping criterion is reached. That is, our alternating optimization algorithm can be conceptually summarized as

$$\{\hat{\mathbf{A}}^{(n+1)}, \hat{\sigma}^{2\,(n+1)}\} = \arg \min_{\mathbf{A}, \sigma^2} f(\hat{\theta}^{(n)}, \hat{\phi}^{(n)}, \mathbf{A}, \sigma^2) \qquad (46)$$

$$\{\hat{\theta}^{(n+1)}, \hat{\phi}^{(n+1)}\} = \arg \min_{\theta, \phi} f(\theta, \phi, \hat{\mathbf{A}}^{(n+1)}, \hat{\sigma}^{2\,(n+1)}) \qquad (47)$$

where $\hat{a}^{(n)}$ is the estimate of a at the nth iteration. Let $\zeta = [\theta^T \, \phi^T \, \text{vec}(\mathbf{A})^T \, \sigma^2]^T$. The gradient of f with respect to the ith element of ζ is

$$\nabla_{\zeta_i} f = \sum_{p=1}^{P} \text{tr}((\nabla_{\zeta_i}\mathbf{R}_p)\mathbf{R}_p^{-1}(\mathbf{R}_p - \hat{\mathbf{R}}_p)\mathbf{R}_p^{-1}). \qquad (48)$$

The ML estimate is obtained by finding the roots of $\nabla_{\zeta_i} f = 0$. When $\zeta_i = \alpha_p = [\alpha_{1,p} \, \alpha_{2,p} \, \cdots \, \alpha_{K,p}]^T$, (48) becomes

$$(\mathbf{F}\circ\mathbf{F}^*)^T(\mathbf{R}_p^{-T} \otimes \mathbf{R}_p^{-1})((\mathbf{F}^*\circ\mathbf{F})\alpha_p + \sigma^2 \boldsymbol{i}_{MN} - \hat{\mathbf{r}}_p) \qquad (49)$$

where

$$\hat{\mathbf{r}}_p = \text{vec}(\hat{\mathbf{R}}_p). \qquad (50)$$

Equating (49) to zero yields

$$\Upsilon_p \alpha_p + \kappa_p \sigma^2 = \tau_p \qquad (51)$$

where

$$\Upsilon_p = (\mathbf{F}^*\circ\mathbf{F})^H(\mathbf{R}_p^{-T} \otimes \mathbf{R}_p^{-1})(\mathbf{F}^*\circ\mathbf{F}) \qquad (52)$$

$$\kappa_p = (\mathbf{F}^*\circ\mathbf{F})^H(\mathbf{R}_p^{-T} \otimes \mathbf{R}_p^{-1})\boldsymbol{i}_{MN} \qquad (53)$$

$$\tau_p = (\mathbf{F}^*\circ\mathbf{F})^H(\mathbf{R}_p^{-T} \otimes \mathbf{R}_p^{-1})\hat{\mathbf{r}}_p. \qquad (54)$$

Grouping (51) for $p = 1, 2, \ldots, P$, we obtain

$$\Upsilon\alpha = \tau \qquad (55)$$

where

$$\Upsilon = [\check{\Upsilon} \; \kappa] \qquad (56)$$

$$\alpha = [\alpha_1^T \, \alpha_2^T \, \cdots \, \alpha_P^T \, \sigma^2]^T \qquad (57)$$

$$\tau = [\tau_1^T \, \tau_2^T \, \cdots \, \tau_P^T]^T \qquad (58)$$

$$\check{\Upsilon} = \text{diag}(\Upsilon_1, \Upsilon_2, \cdots, \Upsilon_P) \qquad (59)$$

$$\kappa = [\kappa_1^T \, \kappa_2^T \, \cdots \, \kappa_P^T]^T. \qquad (60)$$

The LS solution of (55) is then

$$\alpha = \Upsilon^{-1}\tau. \qquad (61)$$

That is, (46) is realized by (61), and we use the ESPRIT estimates of θ, ϕ and α to construct Υ and τ as the first step of the ML estimator. On the other hand, (47) is implemented via K 2-D searches

$$\{\hat{\theta}_k^{(n+1)}, \hat{\phi}_k^{(n+1)}\} = \arg \min_{\theta_k, \phi_k} f(\theta_k, \phi_k, \hat{\theta}_{k^-}^{(n+1)}, \hat{\theta}_{k^+}^{(n)}, \hat{\phi}_{k^-}^{(n+1)}, \hat{\phi}_{k^+}^{(n)},$$
$$\hat{\mathbf{A}}^{(n)}, \hat{\sigma}^{2\,(n)}) \qquad (62)$$

where $\hat{\theta}_{k^-}^{(n+1)}$ denotes $[\hat{\theta}_1 \, \hat{\theta}_2 \, \cdots \, \hat{\theta}_{k-1}]^T$ at the $(n+1)$th iteration and $\hat{\theta}_{k^+}^{(n)}$ represents $[\hat{\theta}_{k+1} \, \hat{\theta}_{k+2} \, \cdots \, \hat{\theta}_K]^T$ at the nth iteration, while $\hat{\phi}_{k^-}^{(n+1)}$ are $\hat{\phi}_{k^+}^{(n)}$ are defined similarly.

5. Simulation results

Computer simulations are conducted to evaluate the performance of the ESPRIT and ML methods for joint DOD and DOA estimation in bistatic MIMO radar. Newton's method is applied for solving (62) in the ML estimator, and five iterations are employed as the stopping criterion because no significant improvement is observed for more iterations. The mean square error (MSE) is assigned as the performance measure:

$$\text{MSE}(\theta) = \frac{1}{KR} \sum_{r=1}^{R} \|\theta - \hat{\theta}_r\|^2 \qquad (63)$$

$$\text{MSE}(\phi) = \frac{1}{KR} \sum_{r=1}^{R} \|\phi - \hat{\phi}_r\|^2. \qquad (64)$$

where $R = 100$ is the number of independent runs, while $\hat{\theta}_r$ and $\hat{\phi}_r$ are the estimates of θ and ϕ in the rth trial. Furthermore, the minimum achievable variance benchmark of CRLB (see Appendix) is included for assessing the algorithm optimality. We properly scale the noise matrices $\{\mathbf{Q}_p\}$ whose entries are circular complex-valued zero-mean white Gaussian variables to produce different signal-to-noise ratio (SNR) conditions. The SNR is defined as

$$\frac{\sum_{m=1}^{MN} \sum_{\ell=1}^{L} \sum_{p=1}^{P} \|\mathbf{F}^H \Lambda_p \mathbf{F}\|^2}{\sigma^2 MNLP}.$$

We fix $M=2$, $N=3$, $K=6$, $d_t = d_r = 0.25$, $\theta = [-70 \; -35 \; -18 \; 15 \; 30 \; 41]^\circ$ and $\phi = [-60 \; -42 \; -21 \; 5 \; 23 \; 43]^\circ$ and the MSE performance under different values of L and P is studied. Note that L represents the number of samples in each pulse. That is, the pulse width is proportional to L and the sampling intervals for different values of L are identical and thus there is no change in bandwidth. Moreover, a larger value of L or P means more temporal information.

In the first test, we set $L=128$ and $P=50$. The results of MSE (θ) and MSE (ϕ) are shown in Figs. 1 and 2, respectively. It is seen that the ESPRIT algorithm provides an suboptimal performance and its MSEs are above the CRLB by more than 5 dB. On the other hand, the MSE of the ML estimator is able to attain the CRLB when SNR ≥ 4.5 dB. This also implies that the ESPRIT performance cannot attain the CRLB since its equivalent aperture has been reduced but it is suitable for initializing the ML scheme. In the second test, the parameters are changed to $L=256$ and $P=50$. The results shown in Figs. 3 and 4 are similar to those in Figs. 1 and 2 except that the threshold SNRs of MSE (θ) and MSE (ϕ) of the ESPRIT and ML algorithms
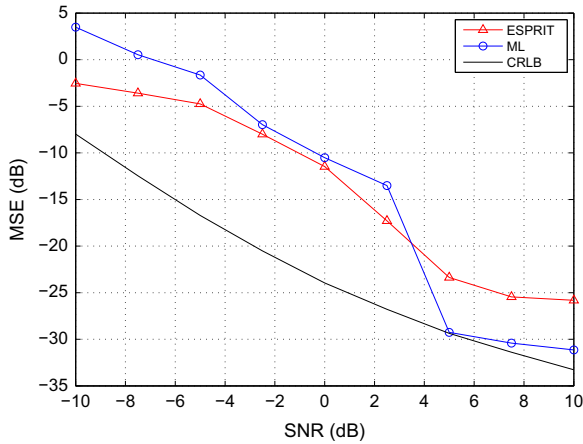
Fig. 1. MSE versus SNR of θ with $L=128$ and $P=50$.
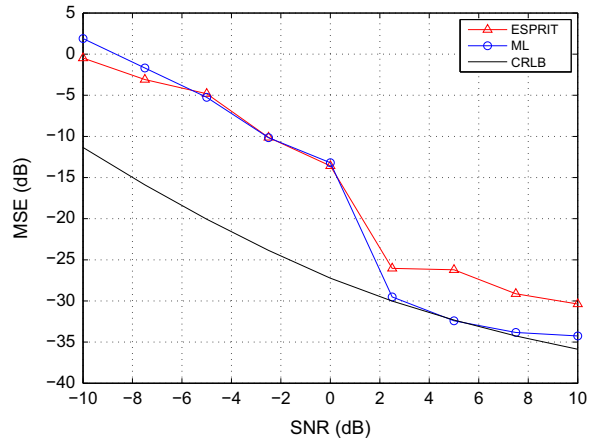
Fig. 2. MSE versus SNR of ϕ with $L=128$ and $P=50$.
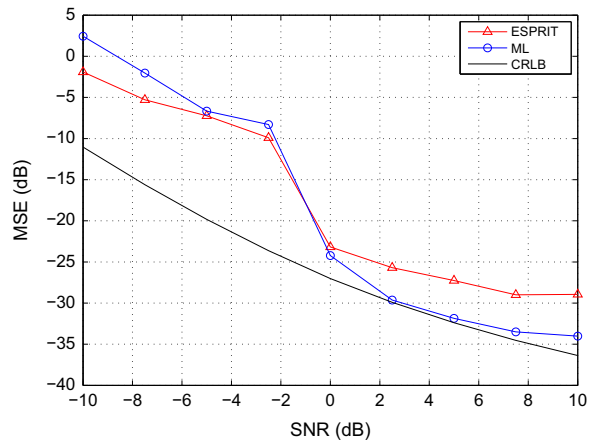
Fig. 3. MSE versus SNR of θ with $L=256$ and $P=50$.

Fig. 4. MSE versus SNR of ϕ with $L=256$ and $P=50$.

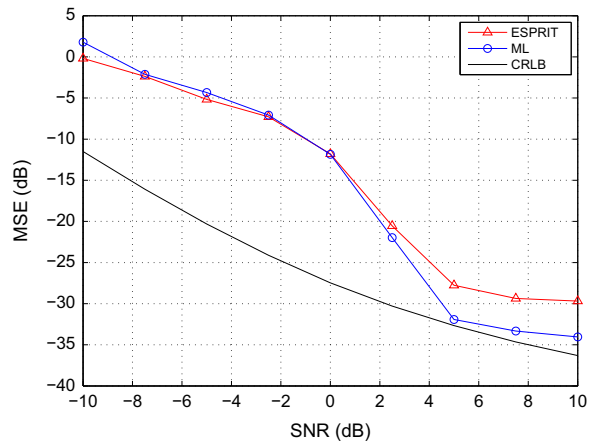**Fig. 5.** MSE versus SNR of θ with $L=512$ and $P=25$.
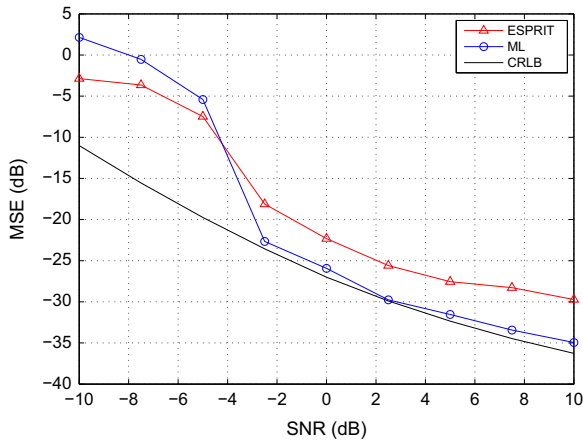
Fig. 6. MSE versus SNR of ϕ with $L=512$ and $P=25$.

change to -2.5 dB and 2.5 dB, respectively. Finally, the scenario of $L=512$ and $P=25$ is investigated. From Figs. 5 and 6, MSE (θ) and MSE (ϕ) of the ESPRIT algorithm are about 7 dB larger than the CRLB. On the other hand, the ML algorithm can attain optimal performance when the SNR is larger than 5 dB. It is worth noting that when the initial

estimates are not sufficiently close to the global solution, local convergence and thus large estimation error will be resulted in the ML method. Hence it has the same threshold performance as that of the ESPRIT method. Nevertheless, it is expected that the former will give

a lower threshold SNR if there is a more accurate initial guess.

6. Conclusion

Two joint DOD and DOA estimation algorithms for bistatic MIMO radar in the presence of white Gaussian noise have been developed. We consider a fast changing environment such that the RCSs vary among pulses. The first is a computationally efficient ESPRIT-like algorithm with suboptimal estimation performance. While the second is the ML estimator which is realized by alternating optimization, and its MSE can attain the CRLB at the expense of higher computational complexity.

Appendix A

The CRLB is derived as follows. The observation vector is $\boldsymbol{x}_\ell = [\mathbf{x}_{1,\ell}^T \ \mathbf{x}_{2,\ell}^T \ \cdots \ \mathbf{x}_{P,\ell}^T]^T$, which is normally distributed with mean $\mathbf{0}_{MNP \times 1}$ and covariance $\mathbf{R}$ in (41). The (m,n) entry of the stochastic Fisher information matrix (FIM) is [21]

$$[\text{FIM}]_{m,n} = L\,\text{tr}((\nabla_{[\boldsymbol{\eta}]_m}\mathbf{R})\mathbf{R}^{-1}(\nabla_{[\boldsymbol{\eta}]_n}\mathbf{R})\mathbf{R}^{-1}) \tag{A.1}$$

where

$$\boldsymbol{\eta} = [\boldsymbol{\theta}^T \ \boldsymbol{\phi}^T \ \text{vec}(\mathbf{A})^T \ \sigma^2]^T. \tag{A.2}$$

As $\mathbf{R} = \text{diag}(\mathbf{R}_1, \mathbf{R}_2, \ldots, \mathbf{R}_P)$ is block-diagonal, (A.1) can be written as

$$\begin{aligned}[\text{FIM}]_{m,n} &= L \sum_{p=1}^{P} \text{tr}((\nabla_{[\boldsymbol{\eta}]_m}\mathbf{R}_p)\mathbf{R}_p^{-1}(\nabla_{[\boldsymbol{\eta}]_n}\mathbf{R}_p)\mathbf{R}_p^{-1}) \\ &= L \sum_{p=1}^{P} \text{vec}^H(\nabla_{[\boldsymbol{\eta}]_m}\mathbf{R}_p)(\mathbf{R}_p^{-T} \otimes \mathbf{R}_p^{-1})\text{vec}(\nabla_{[\boldsymbol{\eta}]_n}\mathbf{R}_p)\end{aligned} \tag{A.3}$$

where the identity $\text{tr}(\mathbf{ABCD}) = \text{vec}^H(\mathbf{A}^H)(\mathbf{D}^T \otimes \mathbf{B})\text{vec}(\mathbf{C})$ has been used. Eq. (A.3) can be written more compactly as

$$\text{FIM} = L \sum_{p=1}^{P} \mathcal{D}_p^H(\mathbf{R}_p^{-T} \otimes \mathbf{R}_p^{-1})\mathcal{D}_p \tag{A.4}$$

where

$$\mathcal{D}_p = \nabla_{\boldsymbol{\eta}^T}\text{vec}(\mathbf{R}_p). \tag{A.5}$$

Let $\mathbf{f}_k = \mathbf{h}_k \circ \mathbf{g}_k$. Then the required terms are calculated as

$$\nabla_{\theta_k}\text{vec}(\mathbf{R}_p) = ((\nabla_{\theta_k}\mathbf{f}_k^*)\circ \mathbf{f}_k + \mathbf{f}_k^* \circ (\nabla_{\theta_k}\mathbf{f}_k))\alpha_{k,p} \tag{A.6}$$

$$\nabla_{\phi_k}\text{vec}(\mathbf{R}_p) = ((\nabla_{\phi_k}\mathbf{f}_k^*)\circ \mathbf{f}_k + \mathbf{f}_k^* \circ (\nabla_{\phi_k}\mathbf{f}_k))\alpha_{k,p} \tag{A.7}$$

$$\nabla_{\alpha_{k,p}}\text{vec}(\mathbf{R}_p) = \mathbf{f}_k^* \circ \mathbf{f}_k \tag{A.8}$$

$$\nabla_{\sigma^2}\text{vec}(\mathbf{R}_p) = \iota_{MN} \tag{A.9}$$

$$\nabla_{\theta_k}\mathbf{f}_k = \mathbf{h}_k \circ (\nabla_{\theta_k}\mathbf{g}_k) \tag{A.10}$$

$$\nabla_{\phi_k}\mathbf{f}_k = (\nabla_{\phi_k}\mathbf{h}_k)\circ \mathbf{g}_k \tag{A.11}$$

$$\nabla_{\theta_k}\mathbf{g}_k = [0 \ e^{j\theta_k} \ 2je^{j2\theta_k} \ \cdots \ j(M-1)e^{j(M-1)\theta_k}]^T \tag{A.12}$$

$$\nabla_{\phi_k}\mathbf{h}_k = [0 \ e^{j\phi_k} \ 2je^{j2\phi_k} \ \cdots \ j(N-1)e^{j(N-1)\phi_k}]^T. \tag{A.13}$$

The CRLB is the inverse of the FIM. Its diagonal elements are the variances of the parameters in $\boldsymbol{\eta}$.

References

[1] J. Li, P. Stoica, MIMO radar with colocated antennas: review of some recent work, IEEE Signal Process. Mag. 24 (5) (2007) 106–114.

[2] A.H. Himovich, R.S. Blum, L.J. Cimini, MIMO radar with widely separated antennas, IEEE Signal Process. Mag. 25 (1) (2008) 116–129.

[3] J. Li, P. Stoica, MIMO Radar Signal Processing, John Wiley & Sons, New Jersey, 2008.

[4] Q. He, R. Blum, A. Haimovich, Noncoherent MIMO radar for location and velocity estimation: More antennas means better performance, IEEE Trans. Signal Process. 58 (7) (2010) 3661–3680.

[5] Q. He, R. Blum, Diversity gain for MIMO Neyman–Pearson signal detection, IEEE Trans. Signal Process. 59 (3) (2011) 869–881.

[6] A. Hassanien, S.A. Vorobyov, A.B. Gershman, Moving target parameters estimation in noncoherent MIMO radar systems, IEEE Trans. Signal Process. 60 (5) (2012) 2354–2361.

[7] R. Xie, Z. Liu, Z. Zhang, DOA estimation for monostatic MIMO radar using polynomial rooting, Signal Process. 90 (1) (2010) 3284–3288.

[8] X.H. Wu, A. Kishk, A. Glisson, Antenna effects on a monostatic MIMO radar for direction estimation, a Cramér–Rao lower bound analysis, IEEE Trans. Antennas Propag. 59 (6) (2011) 2388–2395.

[9] A. Hassanien, S. Vorobyov, Transmit energy focusing for DOA estimation in MIMO radar with colocated antennas, IEEE Trans. Signal Process. 59 (6) (2011) 2669–2682.

[10] B. Friedlander, On signal models for MIMO radar, IEEE Trans. Aerosp. Electron. Syst. 48 (4) (2012) 3655–3660.

[11] M. Jin, G. Liao, J. Li, Joint DOD and DOA estimation for bistatic radar, Signal Process. 89 (2) (2009) 244–251.

[12] B. Tang, J. Tang, Y. Zhang, Z. Zheng, Maximum likelihood estimation of DOD and DOA for bistatic MIMO radar, Signal Process. 93 (5) (2013) 1349–1357.

[13] M.L. Bencheikh, Y. Wang, H. He, Polynomial root finding technique for joint DOA DOD estimation in bistatic MIMO radar, Signal Process. 90 (9) (2010) 2723–2730.

[14] R. Xie, Z. Liu, J. Wu, Direction finding with automatic pairing for bistatic MIMO radar, Signal Process. 91 (1) (2012) 198–203.

[15] D. Chen, B. Chen, G. Qin, Angle estimation using ESPRIT in MIMO radar, Electron. Lett. 44 (12) (2008) 770–771.

[16] J. Chen, H. Gu, W. Su, Angle estimation using ESPRIT without pairing in MIMO radar, Electron. Lett. 44 (24) (2008) 1422–1423.

[17] T. Aittomaki, V. Koivunen, Performance of MIMO radar with angular diversity under Swerling scattering models, IEEE J. Sel. Top. Signal Process. 4 (1) (2010) 101–114.

[18] D. Nion, N. Sidiropoulos, Tensor algebra and multidimensional harmonic retrieval in signal processing for MIMO radar, IEEE Trans. Signal Process. 58 (11) (2010) 5693–5705.

[19] M. Skolnik, Introduction to Radar Systems, McGraw-Hill, New York, 2001.

[20] A.B. Gershman, N.D. Sidiropoulos, Space-Time Processing for MIMO Communications, John Wiley, Chichester, 2005.

[21] P. Stoica, E. Larsson, A. Gershman, The stochastic CRB for array processing: A textbook derivation, IEEE Signal Process. Lett. 8 (5) (2001) 148–150.